Energy Conversion and Management 52 (2011) 2973–2981

Contents lists available at ScienceDirect

Energy Conversion and Management

journal homepage: www.elsevier.com/locate/enconman

Thermal modeling of cylindrical lithium ion battery during discharge cycle

Dong Hyup Jeon *,[1], Seung Man Baek

School of Mechanical and Aerospace Engineering, Seoul National University, Seoul 151-744, Republic of Korea

ARTICLE INFO

Article history:
Received 20 June 2010
Received in revised form 17 March 2011
Accepted 13 April 2011
Available online 7 May 2011

Keywords:
Li-ion battery
Cylindrical
Thermal behavior
Heat generation
FEA

ABSTRACT

Transient and thermo-electric finite element analysis (FEA) of cylindrical lithium ion (Li-ion) battery was presented. The simplified model by adopting a cylindrical coordinate was employed. This model provides the thermal behavior of Li-ion battery during discharge cycle. The mathematical model solves conservation of energy considering heat generations due to both joule heating and entropy change. A $LiCoO_2$/C battery at various discharge rates was investigated. The temperature profile from simulation had similar tendency with experiment. The temperature profile was decomposed with contributions of each heat sources and was presented at several discharge rates. It was found that the contribution of heat source due to joule heating was significant at a high discharge rate, whereas that due to entropy change was dominant at a low discharge rate. Also the effect of cooling condition and the $LiNiCoMnO_2$/C battery were analyzed for the purpose of temperature reduction.

1. Introduction

The development of secondary batteries is presently focusing on the rechargeable lithium-ion (Li-ion) cells for their high voltage and low self-discharge rate [1,2]. The Li-ion batteries attract much interest as an energy storage device since they are capable of providing high energy density and wide range of its application. However high fabrication cost, long-term stability and poor safety characteristics caused by high heat generation during charge/discharge cycles are the challenges [2]. Furthermore excessive temperature rise at a high discharge rate will induce safety issue which may lead to performance degradation and thermal runaway, even the cell burning. In order to scale-up for the automotive application, thermal stability issues must be overcome. An achieving of good battery thermal management would encourage the commercialization of hybrid electric vehicle (HEV) and electric vehicle (EV).

Several recent researches have been studied to understand the thermal behavior of Li-ion batteries by experimental investigation along with numerical simulation. Bernardi et al. [3] described the general energy balance for battery systems by assuming uniform temperature throughout the cell. Doyle et al. [4] developed micro-scale model for the behavior of lithium/polymer/insertion cell under the isotropic condition. Chen and Evans [5], Newman and Tiedemann [6], Pals and Newman [7], Doyle et al. [8], and Thomas and Newman [9] were presented mathematical model focusing on the thermal management. Hong et al. [10] indicated that the entropy change can contribute more than 50% of the total heat generated at the 1 C discharge rate. Srinivasan and Wang [11] studied electrochemical and thermal behavior of Li-ion cells employing two-dimensional unit layer. They found that the effect of heat generation due to entropy is important at all C-rates, especially at low C-rate. The determination of entropy change has been carried out by several researchers. The entropy change of $LiCoO_2$ and LiC_6 was measured by Reynier et al. [12,13], and that of $LiMn_2O_4$ was determined by Kim and Pyun [14], and Yazami et al. [15]. Measuring of thermodynamic properties and entropy changes which are recently available is significantly contributed to the development of thermal management of Li-ion battery. Williford et al. [16] and Viswanathan et al. [17] investigated the effect of entropy changes on the thermal behavior of Li-ion batteries. They pointed out that entropy change of $LiCoO_2$ is larger than the other cathode materials. Pesaran [18] developed lumped capacitance battery thermal model in Matlab/Simulink environment. However he did not describe in details for the mathematical technique. Kim et al. [19] developed thermal abuse model of Li-ion battery by comparing a simple lumped model. Kim et al. [20,21] investigated thermal behavior of Li-ion polymer battery (LIPB). They predicted temperature distribution as a function of potential and current density for the scale-up of the LIPB. However they did not describe how the entropy changes are taken into account on their simulation. Onda et al. [22,23] investigated thermal behavior of Li-ion cylindrical battery. They figured out that temperature may increase above allowable limits during rapid charge/discharge cycles. Inui et al. [24] simulated cylindrical and prismatic Li-ion batteries and validated with experimental results. They modeled commercially available SONY-US18650 cylindrical battery. However they did

* Corresponding author. Address: 301-1414, 599 Gwanak-ro, Gwanak-ku, Seoul 151-744, Republic of Korea. Tel.: +82 2 880 1656; fax: +82 2 883 0179.
E-mail address: dhjeon1@snu.ac.kr (D.H. Jeon).
[1] Present address: Core Technology Lab., Corporate R&D Center, Samsung SDI Co. Ltd., 428-5, Gongse-dong, Giheung-gu, Yongin-si, Gyeonggi-do 446-577, Korea

0196-8904/$ - see front matter © 2011 Elsevier Ltd. All rights reserved.
doi:10.1016/j.enconman.2011.04.013

Nomenclature

A	area, m^2	T	temperature, K or °C
C_p	heat capacity, J/kg K	V	voltage, V
F	Faraday constant, 96,485 C/mol	V^o	open circuit voltage, V
ΔG	gibbs energy change, J/kmol		
h	heat transfer coefficient, W/m K	*Greek letters*	
i	current density, A/m^2	κ	thermal conductivity, W/m K
n	the charge number pertaining to the reaction	ρ	density, kg/m^3
$\dot{q}$	heat generation	σ	electrical conductivity, S/m
ΔS	entropy change		

not consider the effect of each component in the jelly-roll, instead they simplified those as a lumped region. So far, there are a great deal of current research on secondary batteries, especially material characteristics and structures. However relatively little of the literature concentrates on the thermal simulation with commercial Li-ion batteries.

In this study, the thermal behavior of cylindrical Li-ion battery is numerically investigated for the purpose of battery thermal management. The transient and thermo-electric model is incorporated with finite element method (FEM) simulation. This paper provides comprehensive understanding about the thermal behavior of Li-ion battery by illustrating temperature distributions and profiles at various discharge rates. The effects of cooling condition and the $LiNiCoMnO_2$ cathode on the temperature distribution are presented to suggest a temperature reduction.

2. Model description

2.1. Geometry and operating conditions

The Li-ion battery considered in this study is illustrated in Fig. 1. A cylindrical SONY-18650 with 1.5 A h capacity is modeled. The basic unit is composed of spirally-wounded jelly-roll and can. A jelly-roll is embedded within the cylindrical can and is consist of repeating units of five layers: (1) anode, (2) anode current collector (copper), (3) separator, (4) cathode, (5) cathode current collector (aluminum). The other components, i.e., tabs, PTC, insulators, etc., are not considered due to minor effect on the thermal analysis of small-size cylindrical battery. Although the jelly-roll is designed with cylindrically spiral type, we modeled it as round structure for the simplicity of the model. The simplified model enables two-dimensional description of the problems by adopting a cylindrical coordinate as shown in Fig. 2. Since the temperature distribution inside the battery is expected symmetric [24], axisymmetric heat transfer elements are employed for the simulation. A radial boundary conditions at the inside and the convective heat transfer at the outer surface are applied for the boundaries. The geometry details and properties which are collected from open literatures [16,21,25–28] are listed in Table 1.

2.2. Li-ion battery

A typical Li-ion battery uses $LiCoO_2$/C for cathode/anode materials. The electrochemical reactions during the charge/discharge can be expressed as

At positive electrode:

$$Li_{0.5}CoO_2 + xLi^+ + xe^- \underset{\text{charge}}{\overset{\text{discharge}}{\rightleftarrows}} Li_{0.5+x}CoO_2 \quad (1)$$

At negative electrode:

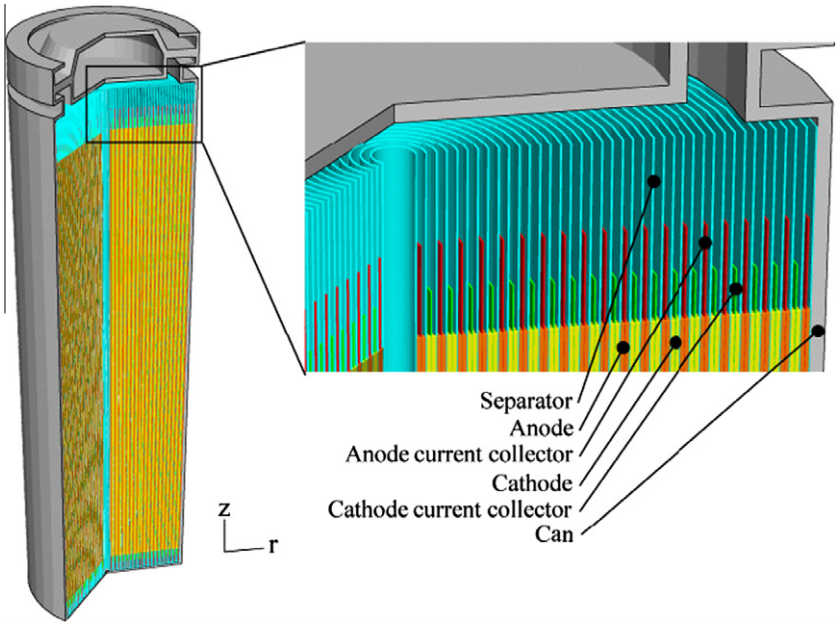

Fig. 1. Schematic illustration of cylindrical Li-ion battery.

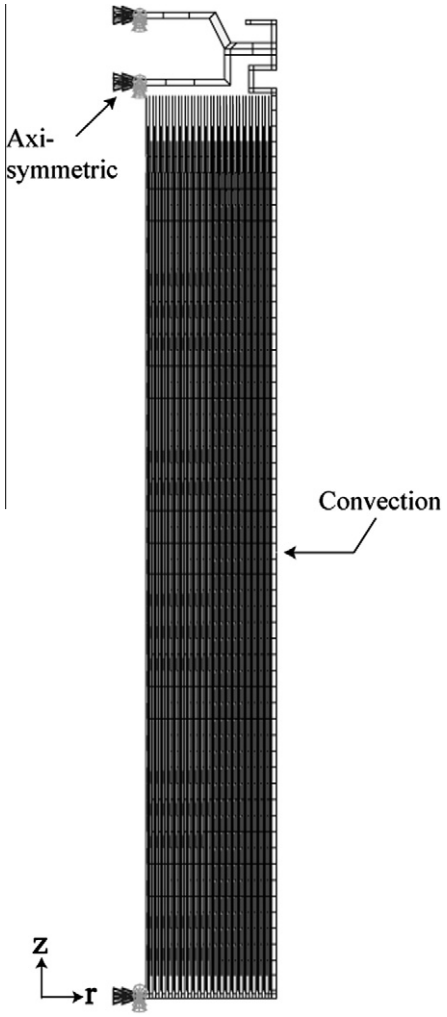

Fig. 2. Numerical model, showing meshes and boundary conditions.

$$LiC_6 \underset{\text{charge}}{\overset{\text{discharge}}{\rightleftarrows}} Li_{1-2x}C_6 + 2xLi^+ + 2xe^- \quad (2)$$

Overall reaction for typical Li-ion battery:

$$2Li_{0.5}CoO_2 + LiC_6 \underset{\text{charge}}{\overset{\text{discharge}}{\rightleftarrows}} 2Li_{0.5+x}CoO_2 + Li_{1-2x}C_6 \quad (3)$$

where the reversible reactions proceed from the left to the right during discharge cycle and the opposite direction occurs during charge cycle. $Li_{0.5}$ is assumed to be 100% state of charge (SOC) of $LiCoO_2$ by following Williford et al. [16]

During discharge cycle, the heat genarations are taken place caused by flowing of current i, through the cell. The heat generation for battery systems which was developed by Bernardi et al. [3] can be written as

$$\dot{q} = i\left(V^o - V - T\frac{\partial V^o}{\partial T}\right) \quad (4)$$

where the term, $i(V^o - V)$, is the heat generation due to joule heating, and the term, $-iT\frac{\partial V^o}{\partial T}$, is the heat generation due to entropy change.

The heat geneartion due to joule heating can be described as

$$\dot{q}_{joule} = i(V^o - V) = \frac{i^2}{\sigma} \quad (5)$$

where $(V^o - V)$ is overpotential.

The heat generation due to entropy change can be written as

$$\dot{q}_{entropy} = -iT\frac{\partial V^o}{\partial T} = -T\Delta S\frac{i}{nF} \quad (6)$$

$$\Delta S = -\frac{\partial \Delta G}{\partial T} = -nF\frac{\partial V^o}{\partial T} \quad (7)$$

where the gibbs energy change is $\Delta G = -nFV^o$.

The entropy changes of $LiCoO_2$, LiC_6 and $LiNiCoMnO_2$ considered in this study are illustrated in Fig. 3. These data are taken from Reynier et al. [12,13] and Williford et al. [16]. It is noticed that the $LiCoO_2$, LiC_6 and $LiNiCoMnO_2$ have negative entropy changes except SOC ≈ 0.9 for $LiCoO_2$ and SOC < 0.15 for LiC_6. A sixth order least-squares polynomial fit to experimental data has been performed as

$$\Delta S_{Li_xCoO_2} = a_0x^6 + a_1x^5 + a_2x^4 + a_3x^3 + a_4x^2 + a_5x + a_6 \quad (8)$$

$$\Delta S_{Li_xC_6} = b_0x^6 + b_1x^5 + b_2x^4 + b_3x^3 + b_4x^2 + b_5x + b_6 \quad (9)$$

$$\Delta S_{LiNi_xCo_yMn_zO_2} = c_0(SOC)^6 + c_1(SOC)^5 + c_2(SOC)^4 + c_3(SOC)^3 + c_4(SOC)^2 + c_5(SOC) + c_6 \quad (10)$$

The corresponding coefficients are reported in Table 2. In order to improve approximation, we divided into several sub-regions. The coefficient of determination, R^2, is used as an indicator of the goodness of approximation. As R^2 indicates, all the empirical equations are close to the data.

By considering the heat generation due to joule heating has a positive value during charge/discharge cycle, the overall discharge reaction can be concluded exothermic.

2.3. Mathematical model

The energy balance equation can be written as

$$\rho C_p A\frac{\partial T}{\partial t} = \nabla(\kappa\nabla T) + \dot{q} \quad (11)$$

$$\dot{q} = \dot{q}_{joule} + \dot{q}_{entropy} = \frac{i^2}{\sigma} - T\Delta S\frac{i}{nF} \quad (12)$$

A surface boundary condition which is dependent on the convective heat transfer is defined as

Table 1
Physical properties of materials.

	Thickness (μm)	Height (mm)	Density (kg/m^3)	Thermal conductivity (W/m K)	Specific heat (J/kg K)	Electrical conductivity ($\times 10^6$, S/m)
$LiCoO_2$	92	53	2291.62	1.85	1.1728	0.0001
$LiNiCoMnO_2$			1500	5	0.7	0.000139
LiC_6	87	53	5031.67	5	0.7	0.0001
Aluminum	10	55	2700	200	0.87	38
Copper	10	57	9000	380	0.381	60
Separator	22	59	1200	1	0.7	–
Can	300	65	7800	16.8	0.478	–

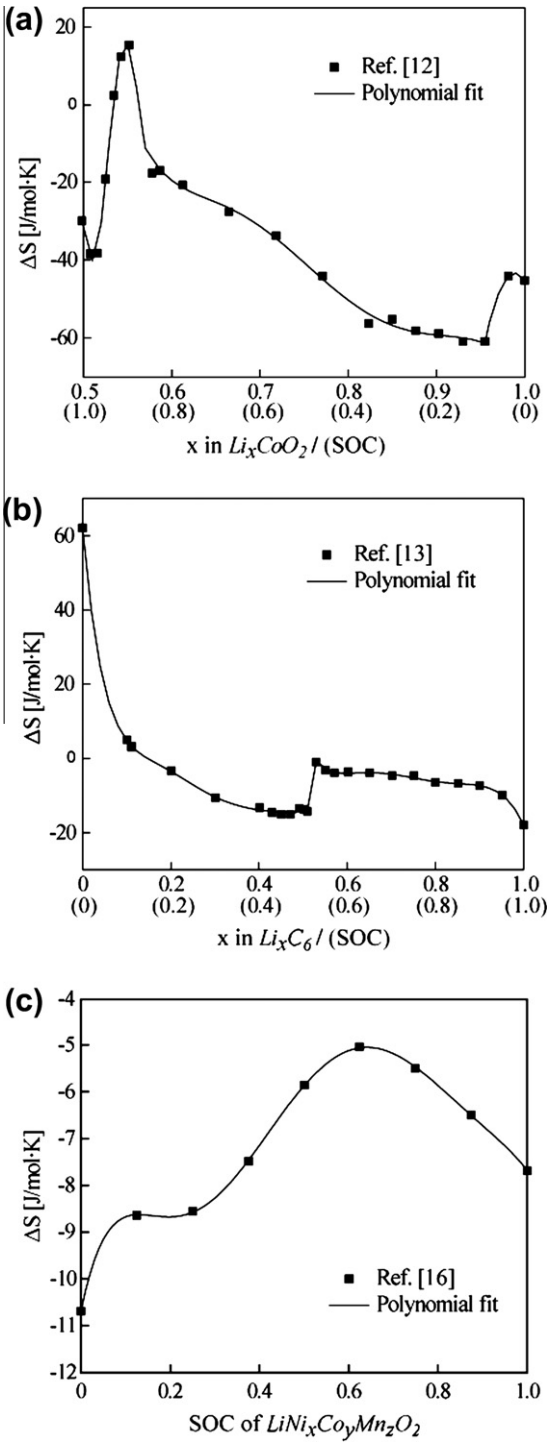

Fig. 3. Entropy changes for (a) $LiCoO_2$, (b) LiC_6, and (c) $LiNiCoMnO_2$ which are taken from Reynier et al. [12,13] and Williford et al. [16].

$$\dot{q}_{convection} = h(T - T_o) \tag{13}$$

where h is the heat transfer coefficient. Using a convective heat transfer coefficient permits to incorporate the effect of different cooling rates at different stages of heat treatment.

Boundary conditions for heat transfer analysis in this study using FE modeling are shown in Fig. 2. Convection heat transfer cooling is beginning from room temperature which is applied on outer surface as 300 K for transient thermal analysis. Although potential gradients are expected along the thickness during discharge, the uniform current generation assumption is considered adequate because the heat generation expression Eq. (4) is developed under the assumption of uniform heat generation throughout the battery system. The left side corresponds to the axis of the axi-symmetric model. The others are considered to be free of any mechanical constraints.

Table 2
Polynomial fit to entropy data.

$\Delta S_{Li_xCoO_2}$			
x	0.5–0.587	0.587–0.955	0.955–1.0
a_0	−11355177040.8594	150923.273	0
a_1	37082724194.5178	−785628.5568	0
a_2	−50400982654.1226	1674586.0981	0
a_3	36492358554.9118	−1872496.991	0
a_4	−14845027870.6635	1159401.9087	−15259.4369
a_5	−3216993522.9774	−377330.3831	30177.8715
a_6	−290133718.7421	50475.9189	−14963.6876
R^2[a]	0.9978	0.9957	1.0
$\Delta S_{Li_xC_6}$			
x	0–0.509	0.509–0.53	0.53–1
b_0	113503.4266	0	15263.1748
b_1	−213472.7565	0	−90131.2904
b_2	160387.7774	0	207733.4471
b_3	−61018.95	0	244004.4274
b_4	12379.2986	0	155717.1982
b_5	−1340.7464	0.106	−51532.5322
b_6	62.0786	0.4756	6936.5109
R^2[a]	0.9996	1.0	0.9962
$\Delta S_{LiNi_xCo_yMn_zO_2}$			
c_0			−496.66
c_1			1729.4
c_2			−2278
c_3			1382.2
c_4			−380.47
c_5			46.508
c_6			−10.692
R^2[a]			0.99989

[a] Closer to 1 indicates better fits.

2.4. Numerical method

The transient simulation in the cylindrical battery was performed by ABAQUS finite element analysis (FEA) solver. The above governing equations are discritized by the finite element method (FEM). The four-node structural and quadratic element plane with axi-symmetric option has been used to model the SONY-18650

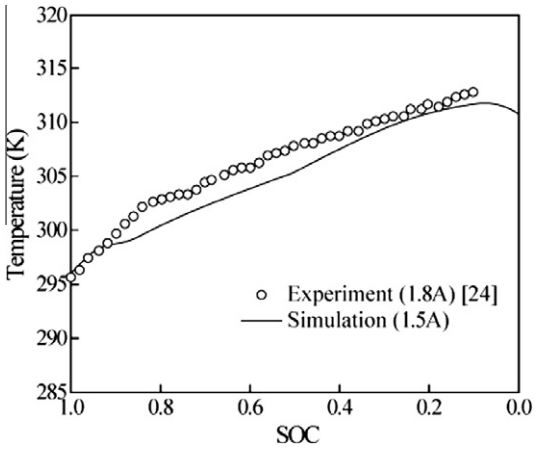

Fig. 4. Comparison between simulation and experiment at a discharge rate of 1 C.

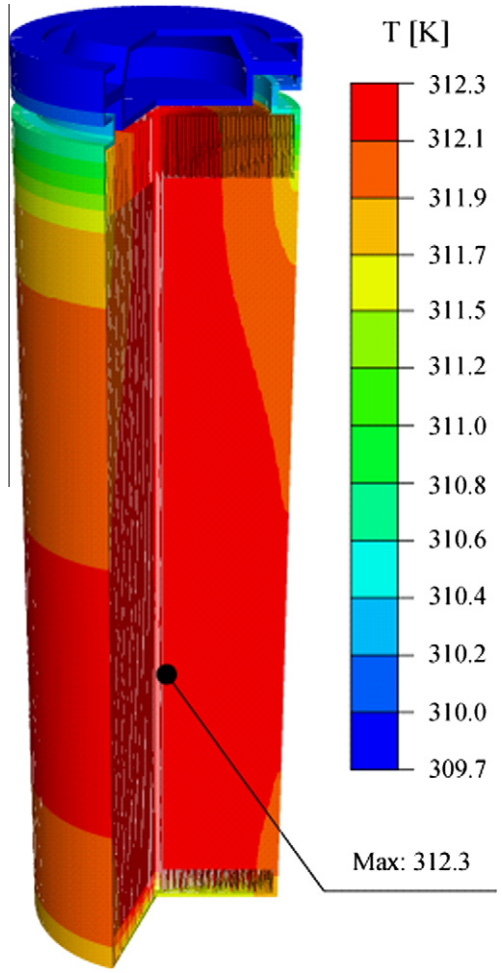

Fig. 5. Temperature distribution of cylindrical Li-ion battery at a discharge rate of 1 C and SOC = 0.1.

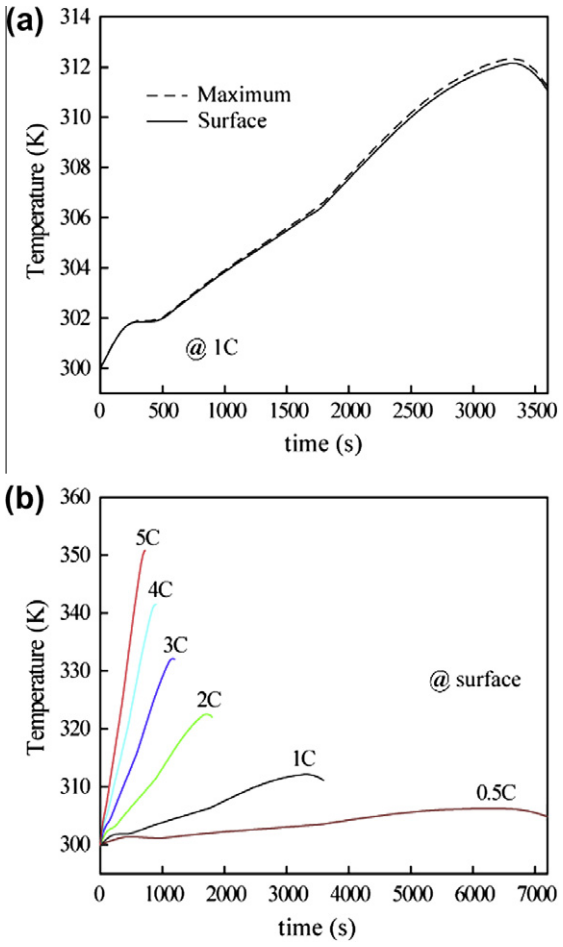

Fig. 6. (a) Comparison of surface temperature and maximum temperature at a discharge rate of 1 C, and (b) surface temperature profiles at discharge rates of 0.5 C, 1 C, 2 C, 3 C, 4 C and 5 C.

battery. The model was meshed with mapped meshing using the quadrilateral-shaped elements. The element size across the plane was uniform since the uniform heat generations are assumed across the area. The fine mesh was imparted at the anodes, cathodes, anode current collectors and cathode current collectors where the heat is generated and it was refined until the results are consistent with only small changes. Time increment satisfying the stability criteria for the constant current discharge is calculated as 1 s. A computer program based on explicit scheme with this time step is developed to compute the temperature field.

3. Results and discussion

The transient FE analysis is performed to investigate the thermal behavior of cylindrical Li-ion battery. SONY-18650 with 1.5 A h capacity that parameters are collected from the literatures is simulated. The battery is operated at constant temperature of 300 K and natural convection heat transfer coefficient of 7.17 W/m K [19]. The heat sources at each components, i.e. anode, cathode, anode current collector, cathode current collector, are taken into account.

3.1. Model validation

The surface temperature of the model is compared with that of the experiment as shown in Fig. 4. Since the data of SONY-18650 with 1.5 A h capacity is not available in the literature, we compare with the experimental result of SONY-18650 with 1.8 A h capacity presented in Inui et al. [24]. The battery is discharged at 1 C rate and the surface temperature is measured at the center of the body. It is observed that the surface temperature of experiment is higher than that of simulation. This is because the battery for experiment has higher capacity than that for simulation. The temperature difference between experiment and simulation is not significant. However the temperature gradient has little discrepancy. This may caused from different material properties and entropy changes according to the changing of capacity. Although the comparison between different capacity batteries is not sufficiently verifiable, we figured out that the simulation result has similar tendency with the experimental data.

3.2. Thermal behavior of Li-ion battery

The temperature distribution of cylindrical Li-ion battery with 1.5 A h capacity is illustrated in Fig. 5. Since the highest surface temperature is presented at SOC = 0.1 as shown in Fig. 4 and the discharge is assumed to be continued until SOC = 0.1 [24] which is correspond to the cut-off voltage, the temperature contour is illustrated at a discharge rate of 1 C and SOC = 0.1. High temperature is observed at the inside of the cell and low temperature is presented at the top cap. The temperature difference between the inside and the outer surface is small. The maximum temperature is found below the center of battery and its rise is 12.3 °C from

Table 3
Predicted temperatures in $LiCoO_2$/C battery at SOC = 0.1.

C-rate	h = 7.17 W/m^2 K			h = 75 W/m^2 K		
	T_{max} (K)	$T_{surface}$ (K)	ΔT	T_{max} (K)	$T_{surface}$ (K)	ΔT
0.5	306.3	306.2	0.1	300.8	300.7	0.1
1	312.3	312.1	0.2	301.6	301.4	0.2
2	322.4	322.1	0.3	304.6	303.9	0.7
3	331.5	331.0	0.5	308.1	307.0	1.1
4	340.3	339.5	0.8	312.3	310.7	1.6
5	348.8	347.8	1.0	317.1	314.9	2.2

the initial temperature. This corresponds well to the result of Chen et al. [29] Moreover the overall appearance of the temperature distribution is good agreement with Inui et al. [24].

Fig. 6 shows temperature profiles at a discharge rate of 1 C. Since it is assumed that the battery is fully charged at the initial state, time = 0 s and 3600 s are corresponds to SOC = 1.0 and 0, respectively. The surface temperature and the maximum temperature are compared in Fig. 6a. The temperature is increased along the discharge time. It is observed that the temperature gradients are changed significantly at time ≈ 330 s, 1800 s and 3300–3600 s, i.e., SOC ≈ 0.9, 0.5 and 0.1–0. This is because the entropy changes are remarkable at SOC ≈ 0.9 for $LiCoO_2$ and SOC ≈ 0.5 and 0.1–0 for LiC_6 as shown in Fig. 3a and b. The maximum temperature is slightly higher than the surface temperature. From Table 3, the temperature difference between the maximum and the surface is increased along the discharge rates. However the differences are very small. This is because the heats are generated across the jelly-roll. The surface temperature profiles at discharge rates of 0.5 C, 1 C, 2 C, 3 C, 4 C and 5 C are shown in Fig. 6b. As discharge rate increases, the surface temperature is raised. For low discharge rate, the surface temperature rise is small and the profiles have paraboloidial shape. However for high discharge rate, the surface temperature is increased significantly and the profiles present linear plot. This is due to contributions of each heat sources which will be discussed in the below.

Fig. 7 shows transient temperature contours at a discharge rate of 1 C. The temperature distributions at discharge times of 360 s, 1080 s, 1800 s, 2520 s, 3240 s and 3600 s, i.e., SOC = 0.9, 0.7, 0.5, 0.3, 0.1 and 0, are presented. At the beginning of discharge, the battery has uniform temperature distribution. It becomes non-uniform as increasing of discharge time due to heat dissipation at the surface. However it is noticed that the temperature non-uniformity across the battery is not significant. Since the heat generation occurs at the jelly-roll, high temperature is observed at the inside of the cell.

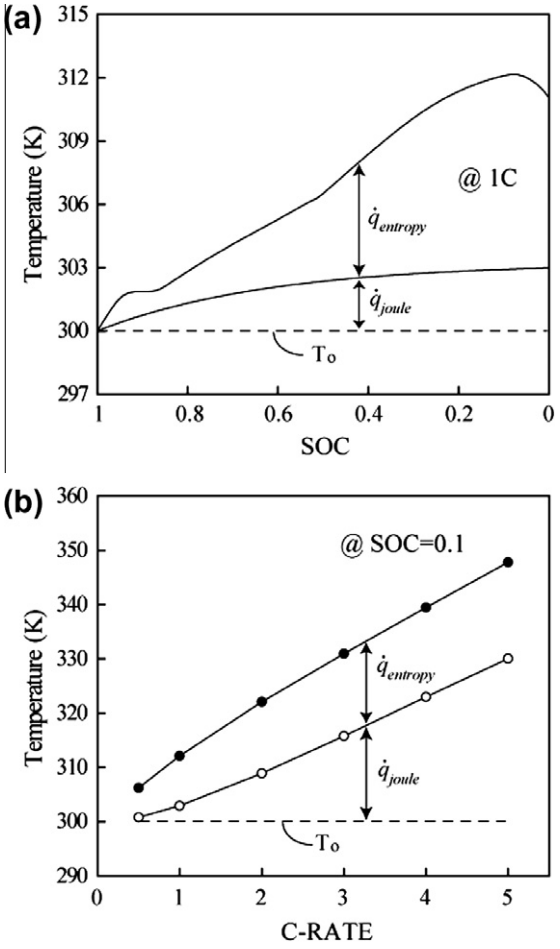

Fig. 8. Surface temperature profile and contribution of each heat sources at (a) a discharge rates of 1 C and (b) SOC = 0.1.

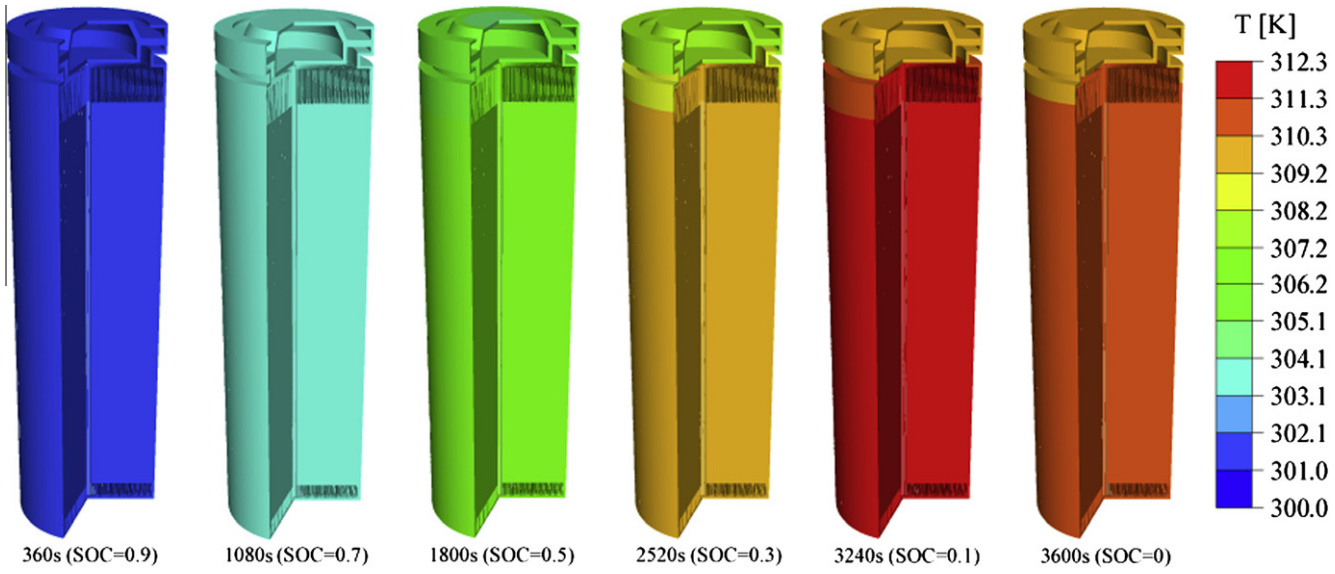

Fig. 7. Simulated sequence of transient temperature contours at a discharge rate of 1 C.

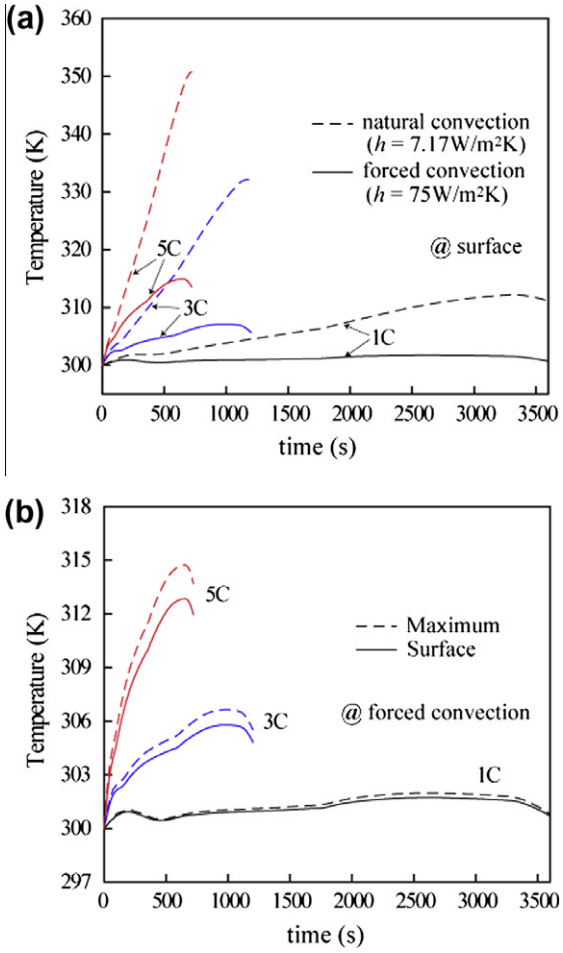

Fig. 9. (a) Surface temperature profiles under different convection conditions and (b) comparison of surface temperature and maximum temperature at discharge rates of 1 C, 3 C and 5 C.

Fig. 8a shows the surface temperature profile and contributions of each heat sources at a discharge rate of 1 C. The contribution of heat generation due to entropy change, $\dot{q}_{entropy}$, is larger than that due to joule heating, $\dot{q}_{joule}$, at a discharge rate of 1 C. For high SOC, the difference between the contributions of $\dot{q}_{joule}$ and $\dot{q}_{entropy}$ is small. However these differences are increased as decreasing of SOC. At SOC = 0.1, the contributions of $\dot{q}_{joule}$ and $\dot{q}_{entropy}$ are estimated 24.1% and 75.9%, respectively. This corresponds well to the result of Hong et al. [10]. It is observed that the contribution of $\dot{q}_{joule}$ become significant at high discharge rates as shown in Fig. 8b. This figure shows the contributions of each heat sources at SOC = 0.1. At a discharge rate of 0.5 C, the contributions of $\dot{q}_{joule}$ and $\dot{q}_{entropy}$ are 12.8% and 87.2%, respectively. However at a discharge rate of 5 C, the contribution of $\dot{q}_{joule}$ is dominant as its amount is 62.8%, whereas the contribution of $\dot{q}_{entropy}$ is decreased to 37.2%. This is because the heat sources are strongly dependent on the current density as $\dot{q}_{joule} \sim i^2$ and $\dot{q}_{entropy} \sim i$ from Eqs. (5) and (6).

3.3. The effect of cooling condition

From the above, a significant temperature rise is expected at high discharge rates, even risking thermal runaway. Cooling the battery could be effective in depressing the temperature. Fig. 9a shows the surface temperature profiles under different convection conditions at discharge rates of 1 C, 3 C and 5 C. A strongly forced convection, i.e., $h = 75$ W/m^2 K which is corresponds to an airflow

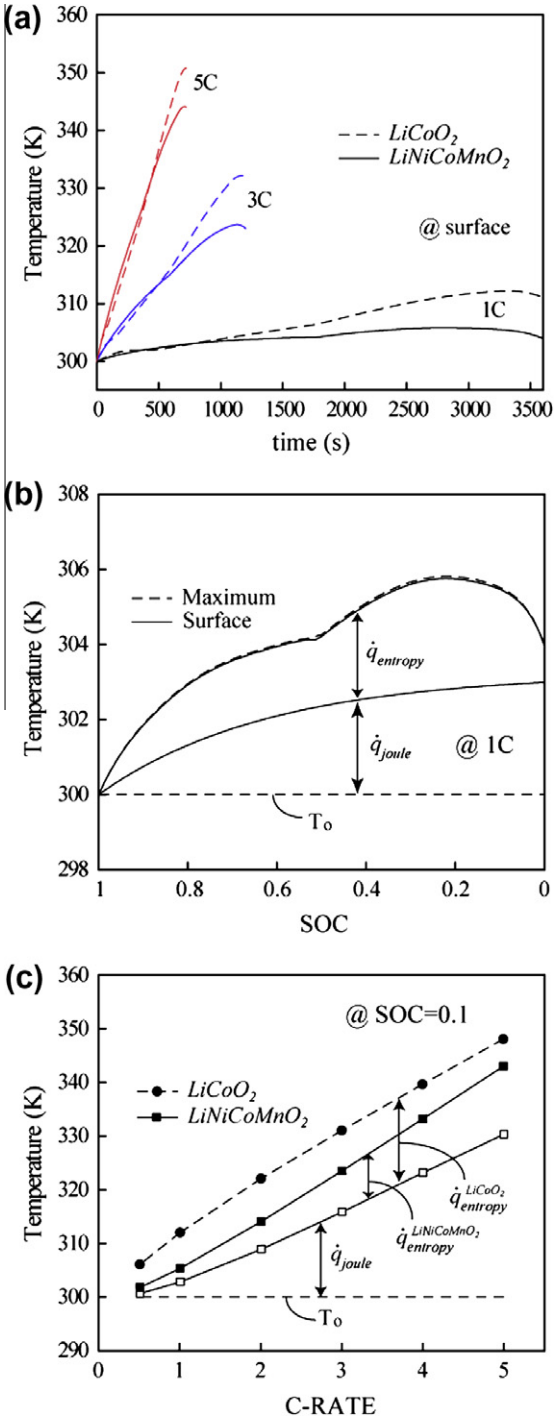

Fig. 10. (a) Surface temperature profiles of $LiCoO_2$/C battery and $LiNiCoMnO_2$/C battery at discharge rates of 1 C, 3 C and 5 C, (b) temperature profiles of $LiNiCoMnO_2$/C battery with contribution of each heat sources at a discharge rates of 1 C, and (c) comparison of $LiCoO_2$/C battery and $LiNiCoMnO_2$/C battery with contribution of each heat sources at SOC = 0.1.

of 35 m/s [30], is employed to investigate the effect of cooling condition. After applying a forced convection, the surface temperature is decreased significantly. For SOC = 0.1, the reduced temperature amounts 88.7%, 77.4% and 68.8% at discharge rates of 1 C, 3 C and 5 C, respectively. However the temperature difference between the maximum and the surface is increased as shown in Fig. 9b. From Table 3, the temperature differences are 0.1 °C, 0.2 °C, 0.7 °C, 1.1 °C, 1.6 °C and 2.2 °C at discharge rates of 0.5 C, 1 C, 2 C, 3 C, 4 C and 5 C, respectively. Compared to the results of natural

Table 4
Predicted surface temperature and contribution of each heat sources at SOC = 0.1.

C-rate	$LiCoO_2$/C			$LiNiCoMnO_2$/C		
	T (K)	$\dot{q}_{joule}$ (%)	$\dot{q}_{entropy}$ (%)	T (K)	$\dot{q}_{joule}$ (%)	$\dot{q}_{entropy}$ (%)
0.5	306.3	12.8	87.2	301.9	41.4	58.6
1	312.3	24.1	75.9	305.4	53.5	46.5
2	322.4	40.4	59.6	314.1	63.3	36.7
3	331.5	51.0	49.0	323.4	67.4	32.6
4	340.3	58.2	41.8	333.0	69.7	30.3
5	348.8	62.8	37.2	342.7	70.3	29.7

convection, the temperature differences between the maximum and the surface are increased high that may result in decreasing of temperature uniformity. Considering that we simulated small-size battery, the thermal management design that minimizes the temperature non-uniformity is required for scale-up to the large-size battery.

3.4. The effect of cathode material

Since the $LiCoO_2$ has much larger entropy change compared to other cathode materials [17], the layered $LiNiCoMnO_2$ materials are widely studied for their excellent safety characteristics due to low heat generation [31]. Although the dimensions on the cathode side could be changed by using $LiNiCoMnO_2$ material, we assumed that the geometry is same as $LiCoO_2$/C battery. Fig. 10a shows surface temperature profile of two different cathode materials at discharge rates of 1 C, 3 C and 5 C, It is compared that surface temperature of $LiCoO_2$/C and $LiNiCoMnO_2$/C batteries. By using $LiNiCoMnO_2$ material on the cathode, the surface temperature is decreased significantly. The reduced amount is similar at each discharge rates as it is 6.7 °C at 1 C, 7.5 °C at 3 C, and 5.1 °C at 5 C. However for the beginning of discharge, i.e., for high SOC, the amount of temperature reduction by using $LiNiCoMnO_2$ cathode is very small, even slightly higher temperature than $LiCoO_2$/C battery at high discharge rates. Fig. 10b shows the temperature profiles of $LiNiCoMnO_2$/C battery and contribution of each heat sources at a discharge rate of 1 C. The temperatures at the maximum and the surface are compared. As discussed in Fig. 6a, the temperature difference between the maximum and the surface is very small. The temperature gradients are changed significantly at time ≈ 1800 s and 2800–3600 s, i.e., SOC ≈ 0.5 and 0.2–0. These are strongly related to the characteristics of entropy change of both anode and cathode materials as shown in Fig. 3b and c. The contribution of $\dot{q}_{joule}$ is similar to that of $\dot{q}_{entropy}$ at a discharge rate of 1 C. For SOC = 0.1, the contributions of $\dot{q}_{joule}$ and $\dot{q}_{entropy}$ are estimated 53.5% and 46.5%, respectively. Compared to the $LiCoO_2$/C battery in Fig. 8a, the contribution of $\dot{q}_{entropy}$ is decreased much due to low entropy changes of $LiNiCoMnO_2$ cathode. Fig. 10c shows the comparison of contributions of each heat sources at SOC = 0.1. It is compared that contribution of $\dot{q}_{entropy}$ in $LiCoO_2$/C and $LiNiCoMnO_2$/C batteries. The temperature of $LiNiCoMnO_2$/C battery is lower than that of $LiCoO_2$/C battery along the discharge rates. This is due to lower contribution of $\dot{q}_{entropy}$ in $LiNiCoMnO_2$/C battery than that in $LiCoO_2$/C battery due to lower entropy change of $LiNiCoMnO_2$ cathode. The different temperature gradients between the two batteries are caused by different material properties. From Table 4, for low discharge rate, it is shown that the contribution of $\dot{q}_{entropy}$ is dominant in LiCoO2/C battery, whereas the contribution of $\dot{q}_{entropy}$ is similar to that of $\dot{q}_{joule}$ in $LiNiCoMnO_2$/C battery. However for high discharge rate, the contribution of $\dot{q}_{joule}$ is considerably high, whereas the contribution of $\dot{q}_{entropy}$ is small. Therefore it can be concluded that the contribution of $\dot{q}_{entropy}$ both in $LiCoO_2$/C and $LiNiCoMnO_2$/C batteries is not significant at high discharge rate. This is because the increasing of heat generation due to joule heating is higher than that due to entropy change at high discharge rate.

4. Conclusion

The cylindrical Li-ion battery was simulated to provide thermal behavior during discharge cycle. The transient model developed a set of energy equations considering heat generations due to both joule heating and entropy change at each cell components. The comparison with experiment indicated the simulation results has similar tendency with the experimental data. For low discharge rate, the highest temperature was observed at SOC = 0.1 caused by the characteristic of entropy changes of $LiCoO_2$ and LiC_6. However for high discharge rate, the temperature was increased linearly along the discharge time and the temperature gradient was steep because the contribution of heat generation due to joule heating is high. The contribution of heat generation due to entropy change was dominant at a low discharge rate, whereas that due to joule heating was significant at a high discharge rate. The maximum temperature was observed inside the cell, but the temperature difference between the maximum and the surface was small.

The battery temperature could be reduced by using cooling system and suitable choice of anode and cathode materials which have lower entropy changes. Cooling the battery with forced convection reduced the temperature significantly, but it also increased the temperature non-uniformity that may degrade the battery performance. Using $LiNiCoMnO_2$ instead of $LiCoO_2$ on the cathode decreased the temperature, but it was effective at a low discharge rate because the contribution of heat generation due to joule heating is significant at a high discharge rate. Although the current collecting tabs were not considered in this model, it could affect on the results in large-size prismatic battery [16] and LIPB [20,21]. In order to scale-up Li-ion cells to large-size battery, thermal stability problems and non-uniform temperature distribution caused by battery cooling should be overcome.

This study described the thermal behavior of Li-ion battery and the methodology is believed to contribute to the battery thermal design.

References

[1] Linden D, Reddy T. Handbook of batteries. 3rd ed. New York: McGraw-Hill; 2001.
[2] Nishi Y. Lithium ion batteries; past 10 years and the future. J Power Sources 2001;100:101–6.
[3] Bernardi D, Pawlikowski E, Newman J. A general energy balance for battery systems. J Electrochem Soc 1985;132:5–12.
[4] Doyle M, Fuller T, Newman J. Modeling of galvanostatic charge and discharge of the lithium/polymer/insertion cell. J Electrochem Soc 1993;140:1526–33.
[5] Chen Y, Evans J. Heat transfer phenomena in lithium polymer-electrolyte batteries for electric vehicle application. J Electrochem Soc 1993;140:1833–8.
[6] Newman J, Tiedemann W. Temperature rise in a battery module with constant heat generation. J Electrochem Soc 1995;142:1054–7.
[7] Pals C, Newman J. Thermal modeling of the lithium/polymer battery. J Electrochem Soc 1995;142:3274–81.
[8] Doyle M, Newman J, Gozdz A, Tarascon J-M. Comparison of modeling predictions with experimental data from plastic lithium ion cells. J Electrochem Soc 1996;143:1890–903.
[9] Thomas K, Newman J. Thermal modeling of porous insertion electrodes. J Electrochem Soc 2003;150:A176–92.
[10] Hong J-S, Maleki H, Al Hallaj S, Redey L, Selman J. Electrochemical–calorimetric studies of lithium-ion cells. J Electrochem Soc 1998;145:1489–501.
[11] Srinivasan V, Wang CY. Analysis of electrochemical and thermal behavior of Li-ion cells. J Electrochem Soc 2003;150:A98–A106.
[12] Reynier Y, Graetz J, Swan-Wood T, Rez P, Yazami R, Fultz B. The entropy of Li intercalation in Li_xCoO_2. Phys Rev B 2004;70:174304.
[13] Reynier Y, Yazami R, Fultz B. Thermodynamics of lithium intercalation into graphites and disordered carbons. J Electrochem Soc 2004;151:A422–6.
[14] Kim S-W, Pyun S-I. Thermodynamic and kinetic approaches to lithium intercalation into a $Li_{1-\delta}Mn_2O_4$ electrode using Monte Carlo simulation. Electrochim Acta 2001;46:987–97.
[15] Yazami R, Reynier Y, Fultz B. Entropymetry of lithium intercalation in spinel manganese oxide: effect of lithium stoichiometry. ECS Trans 2006;1:87–96.

[16] Williford R, Viswanathan V, Zhang J-G. Effects of entropy changes in anodes and cathodes on the thermal behavior of lithium ion batteries. J Power Sources 2009;189:101–7.
[17] Viswanathan V, Choi D, Wang D, Xu W, Towne S, Williford R, et al. Effect of entropy change of lithium intercalation in cathodes and anodes on Li-ion battery thermal management. J Power Sources 2010;195:3720–9.
[18] Pesaran A. Battery thermal models for hybrid vehicle simulations. J Power Sources 2002;110:377–82.
[19] Kim G-H, Pesaran A, Spotnitz R. A three-dimensional thermal abuse model for lithium-ion. J Power Sources 2007;170:476–89.
[20] Kim US, Shin CB, Kim CS. Effect of electrode configuration on the thermal behavior of a lithium–polymer battery. J Power Sources 2008;180:909–16.
[21] Kim US, Shin CB, Kim CS. Modeling for the scale-up of a lithium-ion polymer battery. J Power Sources 2009;189:841–6.
[22] Onda K, Kameyama H, Hanamoto T, Ito K. Experimental study on heat generation behavior of small lithium-ion secondary batteries. J Electrochem Soc 2003;150:A285–91.
[23] Onda K, Ohshima T, Nakayama M, Fukuda K, Araki T. Thermal behavior of small lithium-ion battery during rapid charge and discharge cycles. J Power Sources 2006;158:535–42.
[24] Inui Y, Kobayashi Y, Watanabe Y, Watase Y, Kitamura Y. Simulation of temperature distribution in cylindrical and prismatic lithium ion secondary batteries. Energy Convers Manage 2007;48:2103–9.
[25] Sikha G, White R, Popov B. A mathematical model for a lithium-ion battery/electrochemical capacitor hybrid system. J Electrochem Soc 2005. 152A1682–152A1693.
[26] Ramadass P, Haran B, White R, Popov B. Capacity fade of Sony 18650 cells cycled at elevated temperatures: part I. Cycling performance. J Power Sources 2002;112:606–13.
[27] Baker D, Verbrugge M. Temperature and current distribution in thin-film batteries. J Electrochem Soc 1999;146:2413–24.
[28] Arora P, Doyle M, Gozdz A, White R, Newman J. Comparison between computer simulations and experimental data for high-rate discharges of plastic lithium-ion batteries. J Power Sources 2000;88:219–31.
[29] Chen SC, Wan CC, Wang YY. Thermal analysis of lithium-ion batteries. J Power Sources 2005;140:111–24.
[30] Holman JP. Heat transfer. 6th ed. Singapore: McGraw-Hill; 1986.
[31] He Y-B, Tang Z-Y, Song Q-S, Xie H, Yang Q-H, Liu Y-G, et al. J. Power Sources 2008;185:526.